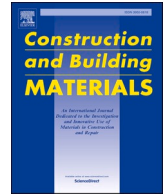




Contents lists available at ScienceDirect

Construction and Building Materials

journal homepage: www.elsevier.com/locate/conbuildmat

Gypsum-based materials for exterior applications using lime and recycled pozzolanic additions

Kerstin Elert^{a,b,*}, María Marta Spallarossa Jiménez^b, Miguel Burgos-Ruiz^b

^a Escuela de Estudios Árabes (EEA-CSIC), Cuesta del Chapiz 22, Granada 18010, Spain

^b Department of Mineralogy and Petrology, University of Granada, Fuentenueva s/n, Granada 18071, Spain

ARTICLE INFO

Keywords:

Gypsum plaster
Mechanical properties
Weathering test
Embodied energy
Pozzolanic additives
Ternary blends

ABSTRACT

Gypsum plaster could replace more energy-intensive building materials, especially considering the versatility of traditional gypsum used for exterior/structural applications since ancient times. However, low weathering resistance limits the exterior use of modern industrial gypsum and suitable additives are required to design optimized plasters and renders. Here, ternary plasters containing 50–95 wt% gypsum and varying amounts of lime and a commercial recycled pozzolanic additive (Metapor®) are compared with pure gypsum plaster to verify whether pozzolanic reaction products are responsible for the often praised superior performance of traditional gypsum. A detailed mineralogical, physico-mechanical, and hygric characterization shows that bassanite hydration is delayed and calcium carbonate polymorphs are stabilized in the presence of additives, while porosity and pore size distribution can be controlled by varying the additive content. Compressive and flexural strength reveal a negative correlation with additive content and a high additive content is required to improve weathering. However, a 25–40 % reduction in embodied energy can be achieved by replacing commonly used metakaolin or Portland cement with Metapor®. Our findings contribute to a better understanding of underlying reaction processes in gypsum-based materials and facilitate a wider use of modified gypsum formulations in sustainable construction and rehabilitation/conservation interventions.

1. Introduction

For more than a decade, significant research efforts in civil engineering and construction have focused on sustainable building materials in order to reduce the industry's carbon footprint [1,2]. Considering the relatively low calcination temperature of gypsum (i.e., calcination T of industrial gypsum being 135–180°C and that of lime and cement being ~900°C and ~1400°C, respectively) and the fact that no CO₂ is released during its transformation into hemihydrate (i.e., hemihydrate, the mineral bassanite, being the raw material for modern industrial plasters, which forms upon partial dehydration of gypsum: $\text{CaSO}_4 \cdot 2 \text{H}_2\text{O} \rightarrow \text{CaSO}_4 \cdot 0.5 \text{H}_2\text{O} + 1.5 \text{H}_2\text{O}$), gypsum would seem a valuable candidate for the design of sustainable building materials and compatible replacement materials for conservation and rehabilitation interventions [2,3]. However, its low weathering resistance and wet-mechanical strength limits exterior and structural applications and makes gypsum the preferred material for interior plastering [4]. Even though differentiation between lime- and gypsum-based materials for exterior and interior applications existed since Roman times [5], traditional gypsum

was applied in a much more versatile manner (i.e., structural and exterior applications for columns, load-bearing walls, slabs, structural ribs, arches, vaults, cantilevered staircases, façades, and floors) as compared to modern gypsum, especially in regions that were in close proximity to gypsum deposits [6]. It has been suggested that the presence of pozzolanic phases could be responsible for the superior quality of traditional gypsum [7,8]. Traditional gypsum is a multiphase product containing uncalcined gypsum, bassanite, and anhydrite (CaSO₄), and quartz, calcite and clays are common accessory minerals in gypsum stone [9]. During calcination in traditional kilns generally higher temperatures are reached (possibly as high as ~1000°C) as compared to those in modern industrial kilns [3,7]. Thus, accessory minerals can undergo transformation as the conversion of calcite into CaO starts at 600°C [10] and the pozzolanic activity of clay minerals such as montmorillonite and kaolinite increases significantly due to dehydroxylation and amorphization after thermal activation [11]. Even though, pozzolanic phases (e.g., hydrated calcium aluminates or hydrated calcium (alumino) silicates) can theoretically form during the hydration of bassanite into gypsum (i.e., $\text{CaSO}_4 \cdot 0.5 \text{H}_2\text{O} + 1.5 \text{H}_2\text{O} \rightarrow \text{CaSO}_4 \cdot 2 \text{H}_2\text{O}$)

* Corresponding author at: Escuela de Estudios Árabes (EEA-CSIC), Cuesta del Chapiz 22, Granada 18010, Spain.

E-mail address: kerstin.elert@eea.csic.es (K. Elert).

<https://doi.org/10.1016/j.conbuildmat.2024.138713>

Received 10 May 2024; Received in revised form 7 October 2024; Accepted 10 October 2024

Available online 13 October 2024

0950-0618/© 2024 The Author(s). Published by Elsevier Ltd. This is an open access article under the CC BY-NC license (<http://creativecommons.org/licenses/by-nc/4.0/>).

containing the aforementioned impurities, unambiguous proof for their existence in traditional gypsum has not been provided so far. This is likely due to the fact that the accessory mineral content is commonly limited [6,8] and the resulting CSH phases are often of amorphous nature, which makes detection with conventional analytical techniques difficult. In order to determine whether pozzolanic phases could improve the weathering resistance of gypsum and enable the design of sustainable plasters and renders, artificial mixtures containing varying amounts of bassanite, quicklime, and a recycled pozzolan (Metapor®) were studied. Previous studies of ternary plasters and mortars mainly used fly ash [12–14] and metakaolin [15–17] as pozzolanic additives but also mixtures of Portland cement and natural pozzolan [18], often in combination with phosphogypsum [19]. However, fly ash production has been in stark decline due to environmental restriction and the reduction in coal-based power generation, while metakaolin and Portland cement have the disadvantage of involving additional energy consumption for the calcination at high T (i.e., 600–700°C for metakaolin, [11]). Here, we evaluate Metapor®, a by-product of the expanded glass industry, as a possible candidate to design optimized, more sustainable gypsum plasters and renders for exterior applications. So far, this recycled product has not been considered for ternary gypsum plasters. In contrast to previous studies, which commonly focused on mixtures with relatively low gypsum content, rarely exceeding 40 wt% [12–14,17,20]), we evaluate the effect of quicklime and pozzolan additions in mixtures with 50–95 wt% gypsum to fill the existing research gap. This evaluation includes a comprehensive compositional and textural characterization in relation to the weathering resistance and mechanical performance of the set plaster, also considering the energy consumption associated with the production of the different plaster mixtures. The outcome of this research not only contributes to a better understanding of the underlying reaction processes in gypsum-based building materials and clarifies whether pozzolanic reaction products are actually responsible for the superior performance of traditional gypsum, but also opens up opportunities for a wider use of modified gypsum formulations in sustainable construction and rehabilitation/conservation interventions (Fig. 1).

2. Materials and methods

2.1. Materials and sample preparation

Reagent grade gypsum (Merck Group, Germany) and local quicklime calcined in traditional kilns at $T > 900^\circ\text{C}$ for 15–20 hours (CaO, Gordillos Cal de Morón S.L.U., Spain) were used for sample preparation. Gypsum was calcined at 100°C for 24 h to obtain bassanite

(β -hemihydrate, $\text{CaSO}_4 \cdot 0.5\text{H}_2\text{O}$), and quicklime was calcined at 800°C for 6 h to eliminate any CaCO_3 , which might have formed upon storage. Calcination yielded pure bassanite (Fig. S1a and c) and lime that contains a small amount of anhydrite (<5 wt%); both materials complying with European standards UNE-EN 13279–1 [21] and UNE-EN 459–1 [22], respectively. A by-product of the expanded glass production (Metapor®, Poraver GmbH, Germany) was used as the pozzolanic additive. During the production process, kaolin is added to finely ground bottle glass in order to avoid particle coagulation and partially transformed into metakaolin. The by-product also contains 10 wt% expanded glass (i.e., glass spheres of up to 50 μm) and small amounts of quartz and feldspars (Fig. S1b and d). Table 1 shows its chemical composition. Even though, comparative studies have revealed that Metapor® might result in ~35 % lower strength when mixed with slaked lime as compared to industrially produced metakaolin [23], it was chosen as an environmentally friendly alternative.

Considering that the water/solid ratio significantly influences the porosity of the gypsum plaster and, subsequently, its mechanical strength [24], tests were performed to determine the minimum amount of water necessary to allow for (almost) complete hydration of the mineral phases and adequate consistency for plaster sample preparation. The water/solid mass ratio was 0.7 for pure bassanite and 2 for pure lime. The water content was adjusted considering the bassanite/lime mass ratio in the mix (Table 2). Small batches (10 g) of dry bassanite, lime, and pozzolan were mixed prior to the addition of deionized water to guarantee that a homogeneous mixture was obtained. Using either plasticine or flexible rubber molds, prismatic ($3 \times 0.7 \times 0.7$ cm, for mechanical testing and porosity measurements) and cylindrical samples ($\varnothing = 2.5 \times 0.5$ cm, for all other tests) of limited size were prepared to achieve a high degree of carbonation in a reasonable amount of time. Curing was performed at 85 ± 3 % RH and $20 \pm 3^\circ\text{C}$ for 28 days. High RH was chosen in order to facilitate hydration and carbonation [25,26]. However, XRD analysis revealed that complete carbonation was not achieved during this period. Curing was prolonged for another 28 days involving daily nebulization of plaster samples with deionized water to speed up carbonation and facilitate hydraulic reactions [26].

2.2. Analytical methods and testing

X-ray diffraction (XRD, X'Pert PRO diffractometer, Malvern Panalytical Ltd., UK) was used to determine the mineralogical composition of raw materials and plasters (powder samples) after 28- and 56-day curing, using the following equipment settings: Cu-K α radiation; Ni filter; 45 kV voltage; 40 mA intensity; exploration range of 3–60 $^\circ 2\theta$ and goniometer speed of 0.05 $^\circ 2\theta$ s $^{-1}$. Mineral phase identification/

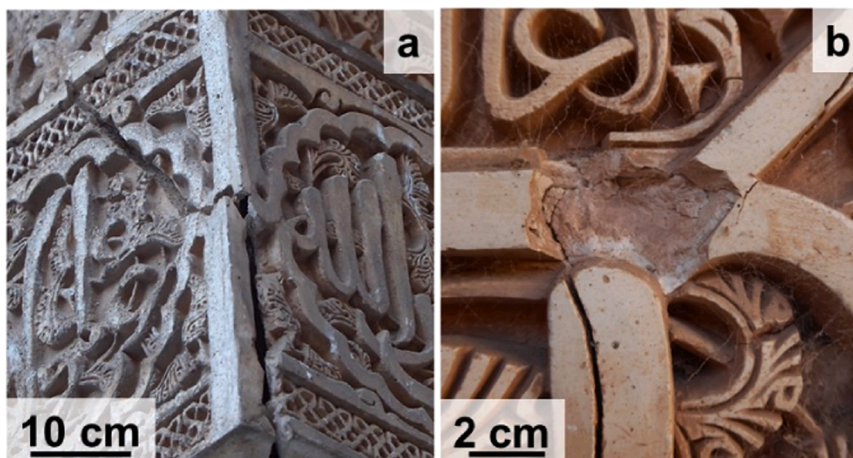


Fig. 1. Images of plasterwork at the Alhambra monument, showing fracturing as well as material loss and evidencing the need for compatible replacement mortars and plasters/renders.

Table 1
Chemical composition of Metapor® based on X-ray fluorescence (XRF) spectrometry (wt%).

SiO ₂	Al ₂ O ₃	Fe ₂ O ₃	MgO	CaO	Na ₂ O	K ₂ O	TiO ₂	P ₂ O ₅	LOI
51.55	31.21	0.34	0.30	2.47	9.48	1.73	0.22	0.19	2.18

Table 2
Composition of plaster mixes (wt%).

Sample	Bassanite	Quicklime	Pozzolan	Water/solid mass ratio
B100	100.0	0	0	0.70
B95	95.0	3.3	1.7	0.73
B90	90.0	6.7	3.3	0.76
B80	80.0	13.3	6.7	0.83
B50	50.0	33.3	16.7	1.02
B0	0	50.0	50.0	1.00

quantification (using experimental reference intensity ratio (RIR) values) and the determination of the gypsum 020/ $\bar{1}$ 21 Bragg peak intensity ratios were performed using HighScore (Malvern Panalytical Ltd., UK) and X Powder software [27]. For each plaster analysis a quarter of a disc-shaped sample was ground in order to obtain a representative bulk sample. Additional XRD analyses were performed to determine the hydration kinetics of the pastes using small batches (i.e., 1 g solid and the corresponding amount of water, Table 2). Immediately after mixing, the pastes were filled into powder sample holders and analyzed. Patterns were collected continuously over a 193.5-min period and an exploration range of 7–45 °2 θ , amounting to a total of 30 successive patterns of 6.45 min duration each (50 % RH, 20 °C). In order to determine bassanite-gypsum conversion in ternary plasters, the initial bassanite content was normalized to 100 % (irrespective of its actual wt% in the mix).

To evaluate the evolution of the carbonation process upon curing, ethanolic phenolphthalein solution was applied by spraying immediately after the disc-shape plaster samples (cured for 28 and 56 days, respectively) were split in half.

Textural and compositional characteristics of carbon-coated raw materials and plasters after 28- and 56-day curing were studied using field emission scanning electron microscopy (FESEM, AURIGA, Carl Zeiss, Germany) coupled with X-ray energy dispersive spectroscopy (EDS, INCA-200, Oxford Instruments, UK). Equipment settings: 10⁻⁶ Pa vacuum and 3 kV acceleration voltage in secondary electron imaging mode and 20 kV acceleration voltage for EDS microanalysis.

Color parameters of plasters after 56-day curing were determined with a spectrophotometer (CM-700d, Konika Minolta, Japan) using the CIE $L^*a^*b^*$ color space (i.e., L^* is luminosity varying from black with a value of 0 to white with a value of 100; a^* varies from + a^* (red) to - a^* (green) and b^* from + b^* (yellow) to - b^* (blue)). Color changes (using pure gypsum plaster as reference) were calculated using the following formula: $\Delta E^* = (\Delta L^{*2} + \Delta a^{*2} + \Delta b^{*2})^{1/2}$. Average values are based on 10 measurements per plaster sample.

A modified version of the procedure described in UNE-EN 15803 [28] was used to determine the water vapor transmission rate (WVTR) of cylindrical plaster samples. Cylindrical plastic containers ($\varnothing = 2.5$ cm and height = 7 cm, filled with 2 mL saturated KNO₃ solution to maintain 93 % RH inside the container) were used instead of the standard cuvette to accommodate the small-sized samples. The seal between sample and container was obtained using plasticine covered with parafilm®. The test was performed in duplicate during 10 days in an environmental chamber at 50 % RH and 23 °C. Obtained results were corrected for phase change-related weight gain during testing due to the formation of calcium carbonate upon carbonation of portlandite (Ca(OH)₂), ettringite, and/or strätlingite using quantitative XRD analysis.

A non-standard accelerated weathering test was used to determine plaster resistance to water impact by spraying. Cylindrical plaster

samples cured for 56 days were placed on a metal grid and sprayed repeatedly on their circular faces with deionized water (300 mL/sample/day) at a distance of 20 cm. Samples were placed in a vertical position so that the water could run off to simulate the effect of rain on a building façade, mimicking mechanical (impact of water droplets) and chemical (dissolution) weathering. Spraying was repeated 14 times over a 3-week period. Samples were dried at 30 °C for 24 h (i.e., until a constant weight was reached) in a ventilated oven between tests to determine weight loss. Tests were performed in duplicate. Weight loss was calculated considering phase change-related weight gain during testing due to carbonation using quantitative XRD analysis.

Total pore volume and pore size distribution of cured plasters were determined with mercury intrusion porosimetry (MIP) using an Auto-pore III 9410 porosimeter (Micromeritics, Norcross, US). This instrument measures pores with 0.003–360 μ m diameter. Samples (~1 g) were dried in a ventilated oven for 48 h at 30 °C prior to analysis. Such low T was chosen in order to avoid temperature-induced phase changes [29].

An Instron 3345 (Instron Co., Canton, US) was used to determine the flexural and compressive strength of plasters after 28 and 56 days of curing using an adapted version of the procedure described in UNE-EN 1015–11 [30]. Prismatic samples (0.5×0.5×4 cm) were tested applying a load of 500 N at 3 mm/min and 5000 N at 6 mm/min for flexural and compressive strength, respectively. Samples were dried in a ventilated oven for 48 h at 30 °C prior to testing. Reported results are based on at least three tests per plaster sample type.

Surface hardness (Leeb hardness [31]) of the plasters cured for 56 days was measured using a durometer equipped with a D-type probe (rebound hammer, PCE-2500N, PCE Instruments, Germany). Reported values are based on a minimum of five tests per sample type.

3. Results

3.1. Mineralogical composition

The mineralogical evolution of plasters was determined using XRD (Fig. 2a, Fig. S1, Table S1). Note that in sample B0 and B50, gypsum-and/or lime-based phases (gypsum, portlandite, and calcium carbonate (CaCO₃) polymorphs vaterite, aragonite, and calcite) are overestimated due to the predominately amorphous character of the pozzolanic additive (i.e., Metapor® containing metakaolin and glass) and the likely presence of some amorphous reaction products (e.g., CS(A)H) in the hydrated plasters. Fig. 2b shows a representative FESEM image of partially dissolved glass spheres with extensive (alkali-induced) corrosion and surface pitting after 56 days of curing. Bassanite hydration kinetics is influenced by the additives, showing a negative correlation with additive content (Fig. 3). Detailed XRD analyses reveal almost complete hydration of the pure bassanite after ~40 min (i.e. 98 % conversion), while 105 and 144 min are required to achieve 95 % hydration in plasters originally containing 95 and 90 wt% bassanite, respectively. Larger amounts of additives further delay hydration and only 68 % conversion is obtained in samples with 50 wt% bassanite after 182 min. XRD analysis also revealed an increase in the intensity ratio of the 020/ $\bar{1}$ 21 gypsum Bragg peaks with increasing additive concentration (Table 3). This trend is more pronounced upon prolonged curing involving water nebulization and has also been observed in samples only containing gypsum and lime [32], indicating a predominantly plate-like morphology due to a relative increase in the area corresponding to the (010) faces of gypsum crystals [33].

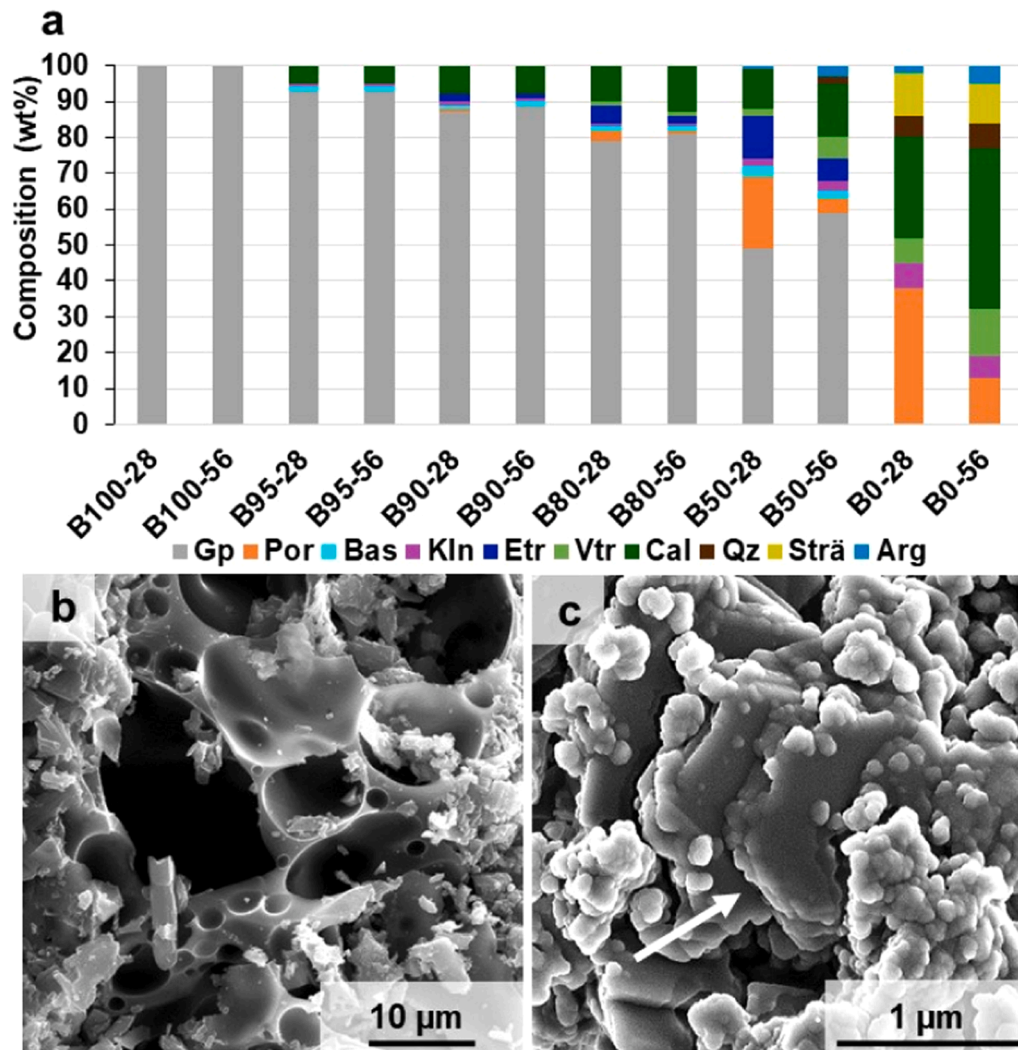


Fig. 2. Mineralogy and microtexture of gypsum-based plasters. a) Mineralogical composition of hydrated plasters after 28 and 56 days of curing based on XRD analysis. Gp = gypsum, Por = portlandite, Bas = bassanite, Kln = kaolinite, Etr = ettringite, Vtr = vaterite, Arg = aragonite, Cal = calcite, Qz = quartz, Strä = strätlingite, b) FESEM image of partially dissolved glass spheres in sample B80 after 56 days of curing, and c) FESEM image of partially dissolved hexagonal plate-like kaolinite crystals (arrow) together with aggregated portlandite and/or calcium carbonate nanoparticles in sample B0 after 28 days of curing.

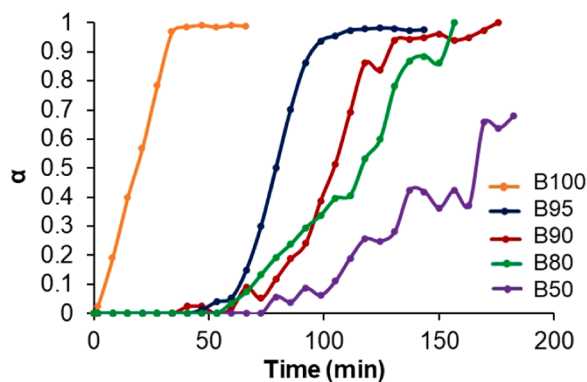


Fig. 3. Fractional conversion (α) of bassanite into gypsum versus time in various plaster mixes based on quantitative XRD analysis.

Experimental results [32] have shown that the hydration of quicklime is fast and 80 % conversion into portlandite is achieved after 10 min. However, portlandite undergoes relatively slow carbonation and after 28 days of curing at 85±3 % RH samples B50 and B0 still

Table 3

Gypsum 020/121 Bragg peak intensity ratio of plasters cured for 28 and 56 days.

Samples	B100	B95	B90	B80	B50
Curing 28 days	0.93	1.02	0.99	1.14	1.12
Curing 56 days	0.98	0.93	1.17	1.23	1.32

contain ≥20 wt% portlandite despite their reduced sample size. Nevertheless, water nebulization proved effective in increasing the degree of carbonation and only 4 and 13 wt% portlandite remain after 56 days in samples B50 and B0. In addition to calcite, vaterite, a metastable calcium carbonate polymorph, is identified in all samples originally containing ≥13.3 wt% quicklime. Furthermore, in samples B50 and B0 small amounts of aragonite, another calcium carbonate polymorph, are detected. The content of both phases increases upon prolonged curing.

Ettringite is present in all samples containing gypsum and pozzolan with the exception of B95, where the amount of ettringite is likely below the XRD detection limit. This hydrous calcium aluminum sulfate mineral (3CaO·Al₂O₃·3CaSO₄·32 H₂O) is a common phase in set Portland cement. Ettringite-based binders are known to reach very high compressive strength but may generate crystallization pressure and cause crack formation upon delayed ettringite formation (70–80 MPa,

[34]). Here, ettringite forms relatively rapidly upon reaction of lime with kaolinite/metakaolin and gypsum and small amounts are already identified after 7 days and its content increases during curing for 28 days, which is in line with findings by Aubert et al. [35]. In sample B0, only containing portlandite and pozzolan, strätlingite ($\text{Ca}_2\text{Al}_2\text{SiO}_7 \cdot 8\text{H}_2\text{O}$) is the major reaction product besides calcium carbonate (i. e., calcite, vaterite, and aragonite). This phase is well-known as a cementing mineral in ancient Roman concrete, claimed to be largely responsible for its extraordinary strength and durability [36]. Strätlingite is a common product phase in metakaolin-lime mixtures [37] and has also been reported together with ettringite for ternary mixtures containing gypsum, lime, and metakaolin [17]. The FESEM image of a plaster sample B0 cured for 28 days (Fig. 2c) shows partially dissolved hexagonal-shaped plate-like kaolinite crystals surrounded by aggregated lime nanoparticles, being the source materials for strätlingite formation. Further curing involving water nebulization results in a significant decrease in the ettringite content in samples containing gypsum. Strätlingite seems slightly more stable, but a reduction in its content is observed after subsequent water vapor permeability testing at high RH (Table S1). This is surprising as significant amounts of unreacted portlandite and kaolinite are still available at the beginning of the permeability test, but no additional strätlingite precipitation is observed and portlandite transforms into calcite (Table S1).

Importantly, harmful salts such as sodium carbonates, bicarbonates,

or sulfates are not detected, which seems reasonable considering the high calcium content, facilitating the precipitation of less soluble calcium carbonate or sulfate. The limited amount of sodium, liberated upon dissolution of the expanded glass in Metapor® at high pH, could theoretically induce the formation of (precursor) zeolitic phases with cementing properties, in particular in samples B0 [38]. However, no such phases are detected with XRD, likely because they are amorphous or poorly crystalline.

3.2. Carbonation

The phenolphthalein test (Fig. 4a and b) confirms XRD data, evidencing almost complete carbonation after 56 days in all samples, with the exception of sample B0 that only reached ~75 % carbonation of portlandite. Samples with high gypsum content show the presence of lime lumps, which have not carbonated and can be identified by their pink color (Fig. 4b, arrows). Remarkably, these samples also suffer bleeding, a process commonly reported for cement-based materials associated with the formation of an aqueous surface layer during curing and phase segregation driven by gravitational forces [39,40]. Consequently, a lime-rich surface layer of ~1–1.5 mm thickness containing mainly portlandite forms in samples B95 and B90. In the case of samples containing larger amounts of additives (B80 and B50), a thick lime-rich layer forms on top of a very thin gypsum-rich layer (0.5–1 mm thick) at

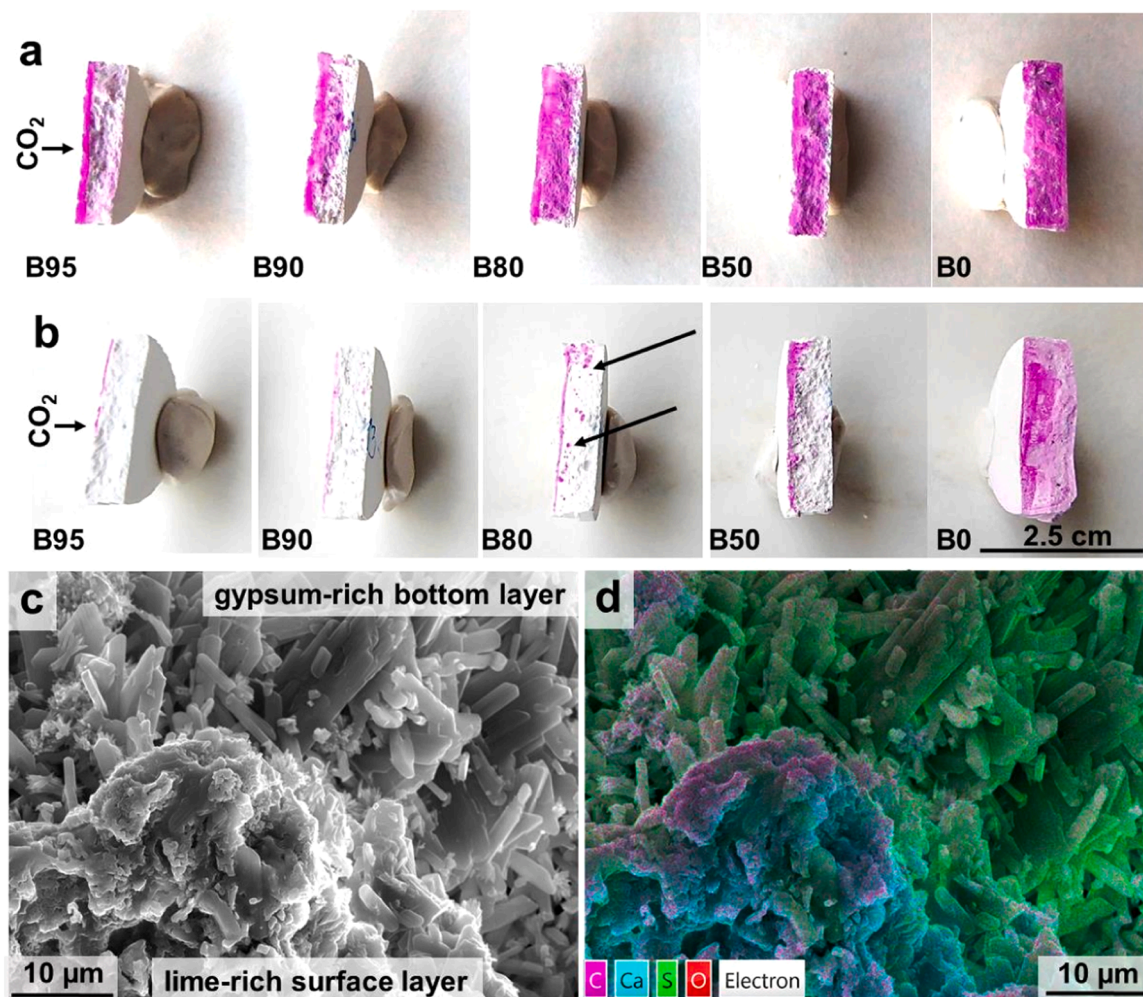


Fig. 4. Carbonation and bleeding. a) and b) Plaster samples after 28 and 56 days of curing, respectively, and subsequent phenolphthalein application immediately after samples were split in half, showing partial carbonation (the dark pink color indicates the presence of portlandite). Some samples contain uncarbonated lime lumps (sample B80, arrows). The direction of the carbonation front is indicated; c) FESEM secondary electron image and d) corresponding elemental map of sample B95 after 56 days of curing, showing phase segregation.

the bottom. Samples containing only lime and pozzolan (B0) show no phase segregation after 28 days of curing as indicated by the homogeneous pink color of the entire cross section. After 56 days, most of the portlandite has undergone carbonation as indicated by the lighter pink color, which is consistent with XRD results.

3.3. Color parameters

Color plays an important role in the case of rehabilitation and conservation interventions. Color measurements (Fig. 5, Table S2) reveal an important change, showing a positive relationship with additive content. A prior study of binary systems containing only gypsum and lime in different proportions revealed no important color variations (i.e., mixtures containing 50 % lime have $\Delta E^* = 0.94 \pm 0.10$, [32]), suggesting that the color change observed here is caused by the addition of the pozzolan, which results in a decrease in luminosity and a shift towards a more yellowish color (i.e., increase in b^*), while a^* hardly changed. In comparison with the pure gypsum plaster, all plasters containing ≥ 20 wt% additive reveal a color change that is perceptible to the human eye ($\Delta E^* = 3$) [41] and the sample B0 has a ΔE^* value above the permissible limit ($\Delta E^* = 5$) for conservation interventions [42]. However, this could be of advantage to match the color of aged historic plasters that commonly display darkening due to soiling over time.

3.4. Porosity and pore size distribution

Based on MIP data, a positive correlation between open porosity and additive content can be established in plasters cured for 28 days (Table 4). However, it has to be kept in mind that the water/solid ratio also increases with additive content (Table 1), the former having a direct influence on the creation of void space according to Yu and Brouwers [24]. The effect seems to have been at play in the case of mixtures with ≤ 20 wt% additives, where relatively small changes in water/solid ratio caused substantial variations in porosity. However, water/solid ratio seems less crucial in blends with higher additive content (i.e., sample B50 and B80 have very similar porosity but the water/solid ratio is substantially higher in the former). Consequently, both parameters (i.e., variations in mineralogical composition and water/solid ratio) have to be considered in the analysis of the pore system. All plasters, with the exception of sample B0, show a bimodal pore size distribution (Fig. 6). The pore diameter of the primary maximum experiences a slight decrease as the additive content increases and is smallest in the gypsum-free sample, being between 1.5 and 2.9 μm . The secondary maximum of the cured plasters is centered at 390 μm , but no clear relation between the volume of large pores (i.e., $>150 \mu\text{m}$) and additive content or water/solid ratio can be established. The gypsum-free sample (B0) reveals an additional broad maximum for pores with 0.15–0.5 μm diameter. Overall, a clear correlation of pozzolan additive content and volume of small pores (i.e., $<0.5 \mu\text{m}$) seems to exist (Table 4), which

Table 4

Porosity and pore size distribution (pore diameter, μm) of plasters with varying amounts of additives cured for 28 days.

Sample	Porosity (%)	Primary max. (μm)	$>150 \mu\text{m}$ (%)	$<0.5 \mu\text{m}$ (%)
B100	34.9	2.9	5.5	2.1
B95	41.3	2.9	10.6	3.2
B90	46.5	2.3	3.7	5.5
B80	51.7	2.3	6.9	7.8
B50	52.4	2.3	4.6	13.1
B0	49.2	1.5	6.0	62.7

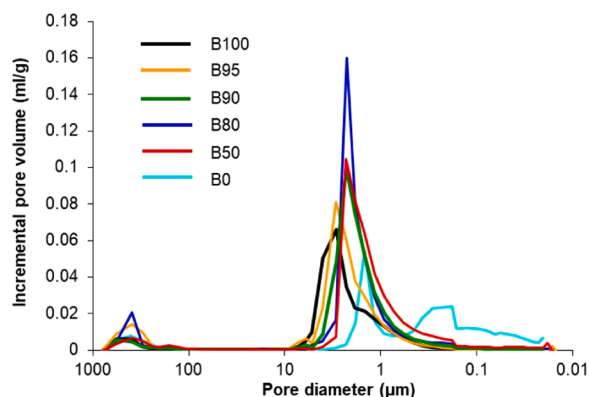


Fig. 6. Pore size distribution (μm) of plasters cured for 28 days.

does not seem to be related to the water/solid ratio (i.e., samples B0 and B50 were prepared using an almost identical water/solid ratio but the former contains almost 5 times more pores with $<0.5 \mu\text{m}$ diameter).

3.5. Mechanical strength and surface hardness

In samples cured for 28 and 56 days, compressive and flexural strength of plaster samples show a negative correlation with additive content (Fig. 7a and b), which has also been observed for binary plasters only containing gypsum and lime [4,32]. None of the ternary plasters containing additives achieves the strength of the pure gypsum plaster, but all plasters fulfill the minimum requirements established for gypsum plaster used for general construction purposes (i.e., compressive strength ≥ 2 MPa according to AENOR [21] and ≥ 5.2 MPa according to ASTM [43], respectively). The mechanical properties of samples B95 remain unchanged upon prolonged curing, which is consistent with the fact that those plasters do not experience any further mineralogical change detectable with XRD (Fig. 7a and b). For comparison, plaster samples containing only lime and pozzolan are included (sample B0) in Fig. 7, which show the highest compressive strength (i.e., 10 % higher strength than the pure gypsum plaster), but comparatively low flexural strength.

Compressive strength values cannot easily be compared with published data for ternary plasters as the preparation parameters (i.e., composition, water/solid ratio, as well as curing conditions and duration) vary greatly, resulting in important data spread. Kumar [12] determined a value of 7–11 MPa for plasters containing 30 wt% gypsum and Marinkovic and Kostic-Pulek [13] reported 7.83 MPa compressive strength for plasters with 40 wt% gypsum, respectively, and varying fly ash/lime proportions. These values are close to those of samples containing 50 wt% gypsum in this study (Fig. 7a). Doleželová et al. [16] found a compressive strength of 20–24 MPa in the case of ternary plasters containing 77 wt% gypsum, while Vimmrová et al. [15] reported 4.75–16.11 MPa for plasters containing 65–85 wt% gypsum and varying lime/metakaolin proportions. The values of the former almost double the compressive strength obtained in this study for samples containing 80 wt% gypsum (Fig. 7a), which is likely related to the lower

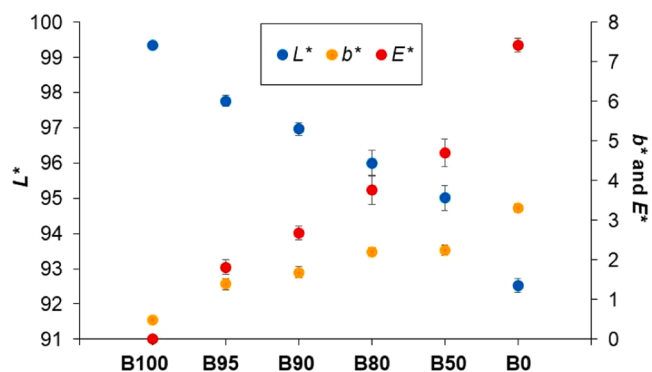


Fig. 5. Color parameter L^* , b^* , and E^* of cured plasters with varying additive content.

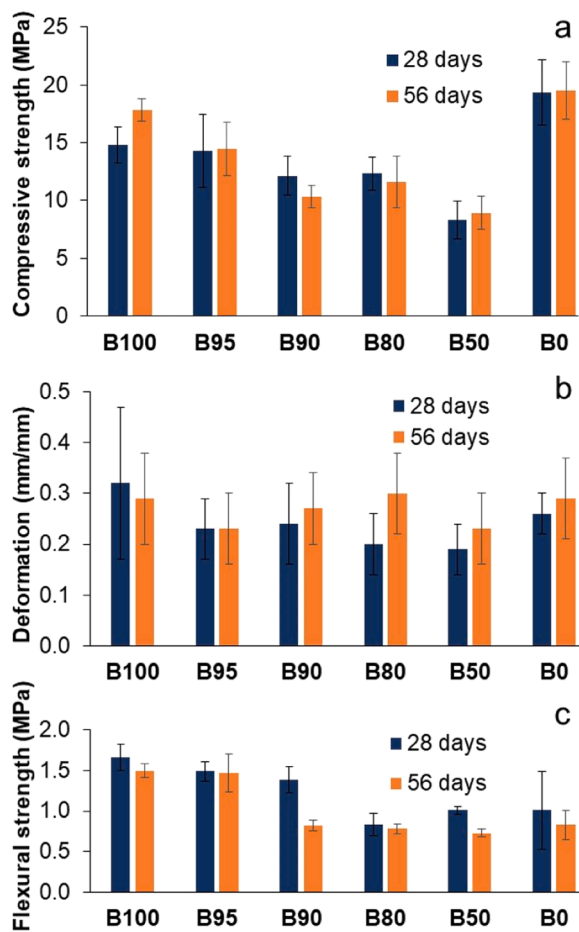


Fig. 7. Compressive strength (a), deformation (b), and flexural strength (c) of plasters with varying lime-pozzolan additions after 28 and 56 days of curing in comparison with pure gypsum plaster (B100), error bars showing standard deviation.

water/solid ratio (0.45–0.5) employed by Doleželová et al. [16]. Murat and Attari [44], in contrast, measured compressive strength values (i.e., 7.4–10.3 MPa) for ternary plasters containing metakaolin, lime and 85–97 wt% gypsum, which are similar to those of this study.

The mineralogical changes undergone upon prolonged curing for 56 days result in a more plastic behavior (i.e., showing higher level of deformation, Fig. 7b) and lower flexural strength in all samples with >10 wt% additive content (Fig. 7c). Pure gypsum samples also experience a reduction in flexural strength, being related to an embrittlement upon prolonged curing as revealed by strain-stress curves. Only samples containing ≤5 wt% additives comply with the minimum requirements for building gypsum according to UNE-EN-13279-1 (flexural strength ≥ 1 MPa [21]) after 56 days of curing, which is in line with findings of our previous study involving gypsum plasters with varying lime content between 5–95 wt% [32]. Unfortunately, only few studies include flexural strength data and reported values show considerable spread. Vimmrová et al. [15] reported 1.81–5.79 MPa for plasters containing 65–85 wt% gypsum and varying lime/metakaolin proportions, while Murat and Attari [45] found flexural strengths of 3.8–4.3 MPa in the case of ternary plasters with 85–97 wt% gypsum. Likely, lower flexural strength values of prismatic samples tested here are at least in part related to the small sample size, where small imperfections (i.e., air voids) likely have a significant impact on strength measurements, especially in the case of the flexural strength testing.

The comparison of compressive and flexural strength of ternary plasters with gypsum-lime plasters (Fig. S3d and e) evidences a positive effect of the pozzolanic additive on compressive strength, in particular

in plasters containing 20–50 wt% additive. In the case of the plasters' flexural strength no clear trend can be identified and a positive effect is only observed in samples B95 and B50.

Surface hardness (Table 5) does not experience important variations upon increase in additive content. It has to be kept in mind that a lime-rich surface layer formed during setting (Fig. 4) in the case of all ternary plasters, and that the Mohs hardness of calcite (Mohs hardness = 3) is only slightly higher than that of gypsum (Mohs hardness = 2). Remarkably, the gypsum-free samples show a 60% higher surface hardness than the pure gypsum plaster, which could be either the result of the substantial strätlingite content [44] or the presence of the unreacted glass portion in the pozzolan (Fig. 2b) with elevated hardness (i.e., glass having a Mohs' hardness of 6.5, while that of kaolinite is only 2–2.5).

3.6. Water vapor permeability

Water vapor permeability results show no clear relation with additive content, the addition of lime and pozzolan leading to variations of 5–13% as compared to pure gypsum (Table 6). It is also not possible to establish any correlation with the plasters' open porosity (Table 4). Indeed, the mixture containing only lime and pozzolan (sample B0) has a similar porosity to that of sample B50 and B80 but shows a substantially lower WVTR, being 21–37% lower than that of the remaining plasters containing gypsum. In this case, the difference in pore size distribution and the large volume of pores with <0.5 μm diameter have to be taken into account as it is well established that pore size as well as pore tortuosity and ambient conditions (i.e., different RH levels in the case of dry- and wet-cup measurements) will influence permeability [46, 47].

3.7. Weathering behavior

Accelerated weathering involving water spraying reveals that a high additive content (i.e., 50 wt%) is required to improve the weathering resistance of ternary plasters and reduce weight loss by ~50% (Table 7). For comparison, samples only containing lime and pozzolan are included, which experienced the smallest weight loss and no surface alteration (Table 7, Figs. 8 and 9a). Samples containing ≤20 wt% additives all suffer similar weight loss after correction for weight gain undergone by the samples due to phase changes based on XRD quantification (i.e., hydration of bassanite and carbonation of portlandite, ettringite, and/or strätlingite; see discussion section below). Remarkably, the formation of a lime-rich surface layer (Fig. 4) does not improve the weathering resistance of these ternary plasters, and surface pitting and material loss can be observed (Fig. 8a). Samples B90, B80, and B50 show surface roughening and the presence of small grains, which were identified as lime lumps using XRD. In the case of the pure gypsum plaster, material loss seems more homogeneous and only some surface pitting is observed (Fig. 8a). The FESEM image (Fig. 9b) provides further insight in the dissolution and recrystallization process undergone by gypsum crystals upon weathering, showing rounded tips and severe corrosion (arrows).

4. Discussion

4.1. Mineralogical and textural evolution

The results of this study reveal a delay in bassanite hydration in the

Table 5

Surface hardness (Leeb hardness) of gypsum-lime-pozzolan plasters after 56 days of curing, including standard deviation.

B100	B95	B90	B80	B50	B0
241 ± 9	242 ± 10	240 ± 28	261 ± 16	245 ± 22	384 ± 14

Table 6

Water vapor transmission rate (WVTR), permeance (W), permeability (δ), resistance factor (μ), and water vapor diffusion-equivalent air layer thickness (S_d) of plasters with varying amounts of additives after 56-day curing, including standard deviation.

Sample	WVTR g/m ³ /day	W (x10 ⁻⁹ kg/ m ² ·s·Pa)	δ (x10 ⁻¹¹ kg/ m·s·Pa)	μ (-)	S_d (m)
B100	243.88 ±1.44	2.33 ±0.01	1.17 ±0.01	17.13 ±0.10	0.086 ±0.001
B95	222.45 ±11.54	2.13 ±0.11	1.06 ±0.06	18.81 ±0.98	0.094 ±0.005
B90	257.14 ±5.77	2.46 ±0.06	1.23 ±0.03	16.25 ±0.36	0.081 ±0.002
B80	276.67 ±2.89	2.65 ±0.03	1.32 ±0.01	15.10 ±0.16	0.076 ±0.001
B50	256.94 ±10.10	2.46 ±0.10	1.23 ±0.05	16.27 ±0.64	0.081 ±0.003
B0	174.01 ±5.77	1.67 ±0.06	0.83 ±0.03	24.03 ±0.75	0.120 ±0.004

Table 7

Weight loss* (wt%) upon accelerated weathering involving water spraying of plasters cured for 56 days, including standard deviation.

B100	B95	B90	B80	B50	B0
19.72 ± 3.12	20.81 ± 2.12	19.63 ± 2.13	19.93 ± 2.81	9.22 ± 0.95	5.60 ± 0.03

* The weight gain (based on quantitative XRD) due to carbonation of portlandite, ettringite, and/or strätlingite, as well as hydration of bassanite is considered.

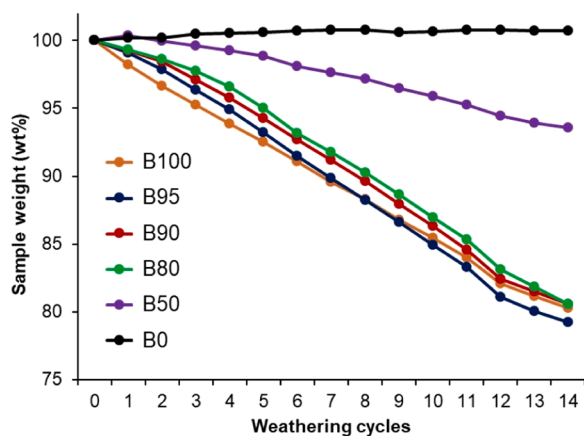


Fig. 8. Evolution of the sample weight during accelerated weathering of plasters cured for 56 days.

presence of lime and the pozzolan additive. This is in line with findings by Karni and Karni [48], suggesting the possible retardation action of lime on bassanite hydration that might be explained by the “common-ion effect” (i.e., quicklime and bassanite share Ca²⁺ as a common cation) [49]. Following Le Chatelier’s principle, the addition of a common ion results in a shift in the chemical equilibrium that is balanced by a reduction in the solubility of salts and other weak electrolytes in the system. Reduced bassanite solubility might, thus, be responsible for the delayed gypsum precipitation in the presence of quicklime [50,51]. However, several other (competing) reactions take place during the hydration setting of ternary plasters and other factors such as pH [52], the presence of magnesium [51,53], as well as the possible formation of a passivation layer could have also played a role in delaying gypsum formation. It is also possible that a small amount of CaSO₄ is incorporated into amorphous (ettringite-type) cementing phases at an early

setting stage, which are not detected with XRD but could have resulted in a slightly reduced gypsum content. Further studies, singling out each potential factor (e.g., titration experiments) are required to determine their effect on gypsum precipitation.

X-ray diffraction also evidenced the stabilization of various calcium carbonate polymorphs in the presence and absence of calcium sulphate. Fernández-Díaz et al. [54] have described the stabilizing effect of sulfates in the case of vaterite, while their stabilizing influence on aragonite is not well established. In a previous work [55], the authors found that aragonite crystallization in 0.05 M Na₂CO₃ aqueous solution was promoted by a high SO₄²⁻/CO₃²⁻ ratio and its transformation into calcite was delayed in the presence of SO₄²⁻ ions. The pozzolanic additive also seems to exert a stabilizing effect on both metastable calcium carbonate polymorphs, especially evident in the absence of calcium sulfate phases (sample B0). This can be attributed to the small amount of magnesium in this additive according to XRF analysis, being known to favor vaterite and aragonite formation and inhibit calcite crystallization [56,57]. Alternatively, it could be argued that silica released upon alkali-promoted dissolution of the glass phase in Metapor® as well as the formation of CSH might have played a role in the stabilization of metastable calcium carbonate polymorphs [58,59].

Prolonged curing or exposure to water vapor during WVTR testing resulted in a decrease in ettringite and strätlingite. This is consistent with the fact that almost complete portlandite carbonation has occurred at this point, leading to a decrease in pH (i.e., the equilibrium pH of portlandite and calcium carbonate being 12.4 and ~9, respectively). Both hydrous phases are known to undergo carbonation (i.e., suffering decalcification) as the pH of the system decreases, giving way to calcium carbonate and/or alumina/silica gel and gypsum [25]. According to Ghorab and Kishar [60] and McCague et al. [61], ettringite and strätlingite are unstable at pH ≤ 11. These results cast doubts about the role played by strätlingite on the durability of Roman concrete [62]. However, they also prove that deleterious delayed ettringite formation does not take place in the studied ternary plasters. Various studies [25, and references herein] show that not only calcite, but also vaterite and aragonite (together with amorphous calcium carbonate as a precursor) are often formed upon carbonation of hydrated calcium silicate phases, which would explain the significant increase in vaterite and aragonite during prolonged curing. However, metastable phases (vaterite and aragonite) will eventually transform into the thermodynamically stable calcite phase as evidenced by the decrease in vaterite during water vapor permeability testing, vaterite being the least stable calcium carbonate polymorph. The transformation process is accompanied by volume and morphology changes, which could theoretically influence strength and durability of ternary plasters and renders. Here, however, such effects have not been observed.

The observed phase segregation might depend on several factors such as the plaster’s drying kinetics influenced by environmental conditions, the mix proportion, and the properties of constituents [63]. Indeed, hydration is much faster in the case of CaO and ~80 % hydration is obtained after only 10 min, while bassanite takes 44 min to reach the same degree of hydration [32]. Moreover, the resulting portlandite crystals are generally much smaller (i.e., < 1–2 μm in size), while gypsum crystals often exceed 10 μm in length, the density of portlandite being slightly lower than that of gypsum (i.e., 2.23 and 2.36 g/cm³, respectively). All these characteristics will have an influence on the observed phase segregation and explain the formation of a lime-rich surface layer.

Findings of this study show that porosity and pore size distribution can be effectively controlled by varying the additive content. Considering the relatively wide range of (open) porosity values reported for historic renders in plasters (i.e., 34 % – 52 % [9,64]), it appears feasible to design plasters that fulfil compatibility requirements for replacement materials for conservation and rehabilitation interventions. However, a high additive content results in an increase in small pores (< 0.5 μm diameter), which might negatively influence durability as demonstrated

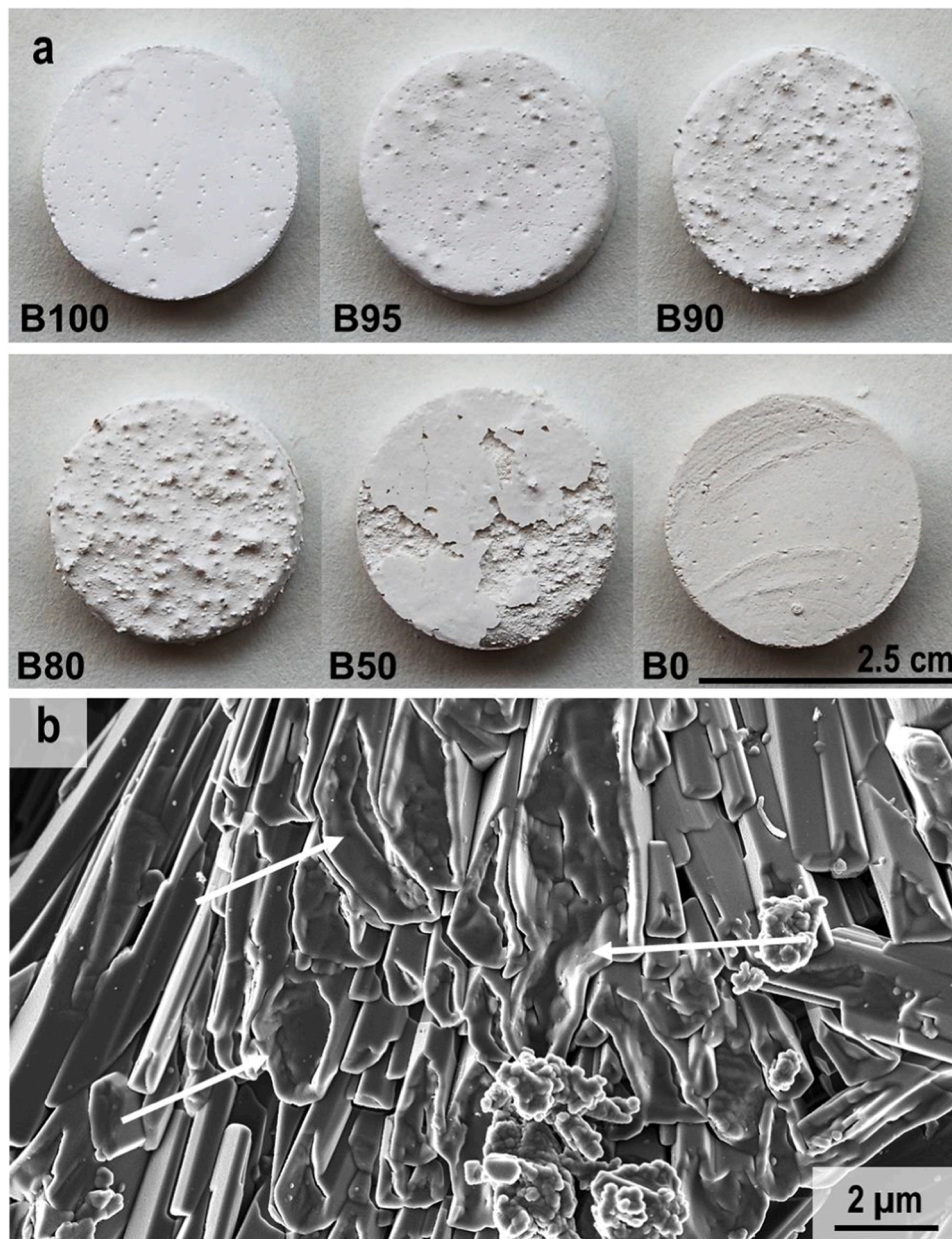


Fig. 9. Weathering test. a) Aspect of disc-shaped plaster samples (cured for 56 days) after weathering involving water spraying. Grains visible in B95, B90, B80, and B50 correspond to lime-rich particles according to XRD analysis. b) FESEM image of sample B95 showing partial dissolution and corrosion (arrows) of gypsum crystals upon accelerated weathering.

by Rodriguez-Navarro and Doehne [65] for other porous substrates. This could be an issue of concern, particularly in the case of the gypsum-free plaster. It could, however, also be of advantage for certain conservation/rehabilitation interventions as these plasters could act as a sacrificial layer (e.g., by selecting plasters with high open porosity and a large volume of small pores to promote salt crystallization in replacement plasters and prevent salt damage to original building materials).

4.2. Strength evolution and water vapor permeability

Pure gypsum samples show higher compressive strength than ternary plasters and experience a 20 % strength increase upon prolonged curing for 56 days that, according to Middendorf [4], could be related to a densification of the plaster matrix due to dissolution-precipitation processes. SEM images of a previous study [32] evidenced surface roughening and crystal aggregation after prolonged curing involving water

nebulization, which could explain the observed improvement in mechanical strength.

The reason for lower strength of ternary plasters seems twofold: i) an increase in additive content requires a higher water/solid ratio during sample preparation (Table 2), which is known to have a negative effect on mechanical properties as it controls the porosity and ultimately the strength of the cured plasters [24], and ii) variations and changes in crystal morphology and mineralogy also seem to affect strength, in particular, upon prolonged curing involving water nebulization. Strength evolution of ternary plasters shows, however, no clear tendency upon curing because various (competing) chemical reactions are at play, leading to mineralogical changes that can have opposing effects on the compressive strength development. Overall, values show relatively high standard deviation, complicating a comprehensive data analysis. Bassanite hydration is generally associated with the formation of a matrix of well interlocked elongated prismatic gypsum crystals,

leading to high strength. However, the presence of additives influences the crystal habit as evidenced by an increase in the 020/ $\bar{1}$ 21 gypsum Bragg peak intensity ratio (Table 3), suggesting the formation of more plate-like, blocky crystals with less capacity to form a well interlocked matrix as reflected by the decrease in compressive strength in plasters with additives. Nevertheless, this strength reduction is probably in part counteracted by the formation of ettringite, the positive effect on the mechanical properties of these needle-shaped crystals being long known [18, and references herein]. Upon further curing, ettringite decomposition is observed, which, nevertheless, does not necessarily lead to a decrease in compressive strength. Indeed, samples containing 50 wt% additive (B50) reveal a small strength gain after 56 days of curing, likely related to the formation of additional gypsum upon ettringite decomposition (Table S1). In the absence of gypsum (B0), the formation of strätlingite seems to be essential to obtain high compressive strength (~20 MPa) as such high mechanical resistance is commonly not achieved in plasters containing mainly calcium-carbonate polymorphs (see below).

Portlandite carbonation does not appear to play an important role in improving mechanical properties. Indeed, samples containing 20 wt% additive (B80) show no improvement in compressive strength despite the formation of additional calcite upon prolonged curing. To this respect the comparatively low compressive strength of lime plaster (<10 MPa) as compared to gypsum plaster has to be considered [4,32,66]. However, possible (limited) strength gain will depend on the polymorph formed upon carbonation. In some samples a significant amount of vaterite forms upon carbonation that will likely not contribute to a significant increase in strength considering the spherical habit of this phase [67]. Aragonite, in contrast, having a needle-shape habit, is known to improve strength in cement [68] and could be responsible for the slight strength increase in samples containing 50 wt % additive (B50). It might also have compensated the potential strength loss due to limited strätlingite carbonation upon prolonged curing in samples containing only lime and pozzolan (B0) (Table S1).

Water vapor permeability of ternary plaster does not vary greatly and is close to that of pure gypsum. Their diffusion resistance factor value (μ , representing the ratio of the diffusion coefficients of water vapor in air and in the building material) is close to that reported by Doleželová et al. [16] for ternary plasters with 77 wt% gypsum (i.e., 18.85). In order to facilitate water transport (in liquid or vapor form) and avoid the creation of a barrier that could accelerate damage due to scaling, restoration renders and plasters should have similar water vapor permeability to the original material [9,69]. Suitable rendering and plastering mortars should have a resistance factor (μ) ≤ 15 according to UNE-EN 998-1a [70]. Note that this standard refers to lime-rich materials but no such standard is available for plasters with high gypsum content. With the exception of sample B0, all ternary plasters reveal resistance factor close to the specified value. The vapor permeability (S_d) values of all ternary plasters, with the exception of samples B0, fall also within the range reported for historic gypsum plasters by Freire et al. [9] (i.e., 0.050–0.094 m), suggesting that compatible materials for rehabilitation and conservation interventions could be designed by varying the gypsum/additive ratio as shown here.

4.3. Energy consumption

Calculations related to energy consumptions were performed taking into account published data of the embodied energy of the various building materials, which were compared to the estimated embodied energy of Metapor®. Considering published embodied energy values for metakaolin (Table 8), it is evident that energy consumption could be reduced by 25 % by replacing this pozzolanic additive with Metapor® in ternary plasters and renders. The results of this study reveal that up to 50 wt% of the lime-pozzolan mixture can be replaced with gypsum to produce ternary plasters with improved weathering resistance and

Table 8

Embodied energy (MJ/kg) of building materials and plaster mixtures.

Material	Embodied energy (MJ/kg)	Ref.
Cement	6.2*	[71–73]
Metakaolin	2.7*	[74]
Lime	5.3*	[72,75,76]
Gypsum (plaster)	2.9*	[72,77]
Metapor®	2.0**	
B100	2.9	
B95	3.0	
B90	3.0	
B80	3.2	
B50	3.6	
B0	3.7	

* average values

** to estimate MJ/kg of Metapor®, the embodied energy of metakaolin without the energy consumption for calcination (i.e., 0.7 MJ/kg [73]) has been considered.

reasonable strength. These ternary plasters (B50) as well as binary plasters (B0) containing lime and Metapor® have the potential to substitute cement-based plasters and renders, facilitating a reduction in energy consumption of ~40 % and, thus, offering a more sustainable alternative to conventional building materials.

5. Conclusion

Findings of this study show that only a high additive content (50 wt % lime and pozzolan) is able to significantly improve weathering resistance of ternary plasters. Furthermore, cementing phases such as ettringite and strätlingite formed upon curing undergo decomposition due to carbonation over time if exposed to high RH environments. Thus, it seems not very likely that the formation of pozzolanic reaction products is responsible for the often reported superior performance of traditional gypsum. However, the additive content has been proven to control bassanite hydration according to our hydration kinetics study. It thus appears feasible to design ternary plasters for specific application by selecting an adequate additive content to adjust their setting behavior and physico-mechanical properties (e.g., open porosity, pore size distribution, and compressive strength). In the context of practical plaster application, the phase segregation phenomenon and inhomogeneous additive distribution (lime lumps) have to be studied further, especially in relation to surface roughening upon weathering to avoid these aesthetic deficiencies.

In comparison with pure gypsum plaster, strength loss has to be expected in the case of ternary plasters, even though, all fulfill common compressive strength requirements. Both, increased water/solid ratio as well as changes in the mineralogical composition, seem to contribute to the strength decrease. Thus, further studies involving plaster mixtures with varying additive content and constant water/solid ratio would be necessary to unambiguously identify the key parameter for strength development (i.e., variations in water/solid ratio or mineral composition). Strength testing also reveals significant variations due to phase changes or embrittlement upon long-term curing, suggesting that the commonly accepted standard curing period of 28 days might not be sufficient to adequately characterize mechanical properties. Importantly, the precipitation of harmful, soluble alkali carbonates and sulfates or deleterious delayed ettringite formation is not detected in ternary plasters. Nonetheless, additional salt leaching tests should be performed to guarantee the innocuousness of the ternary plasters, particularly when applied for built heritage conservation.

Finally, the commercial recycled pozzolanic additive Metapor® proves to be a suitable replacement for industrially produced metakaolin. Binary plasters and ternary plasters with high additive content, prepared using gypsum and/or Metapor® and lime, show improved weathering resistance and reasonable compressive strength (9–20 MPa), with the advantage of utilizing an industrial by-product that, as

compared to industrially produced metakaolin, does not require additional energy for its calcination.

Funding

This research was the topic of the master thesis of M.M. Spallarossa Jiménez (Master Ciencia y Tecnología en Patrimonio Arquitectónico, University of Granada (UGR)). This research was financed by the Unidad de Excelencia “UCE2018-01 - Ciencia en la Alhambra” (UGR), Unidad Científica de Excelencia “UCE.PP2016.05” (UGR), the Research Group “RNM0179” (Junta de Andalucía), and projects PID2023-149367NA-I00 and PID2021-125305NB-I00 (Ministerio de Ciencia, Innovación y Universidades, Spain). K. Elert is a postdoctoral Research Fellow (Ramón y Cajal contract, Ministerio de Ciencia, Innovación y Universidades, Spain).

CRedit authorship contribution statement

María Marta Spallarossa Jiménez: Writing – review & editing, Visualization, Investigation. **Miguel Burgos-Ruiz:** Writing – review & editing, Supervision, Investigation. **Kerstin Elert:** Writing – review & editing, Writing – original draft, Visualization, Supervision, Resources, Project administration, Methodology, Investigation, Funding acquisition, Conceptualization.

Declaration of Competing Interest

The authors declare that they have no known competing financial interests or personal relationships that could have appeared to influence the work reported in this paper

Acknowledgements

We thank Dr. C. Rodríguez-Navarro and four anonymous reviewers for their insightful comments and suggestions. We also thank Dr. C. Benavides-Reyes for her help with strength measurements. SEM analysis was performed at the Centro de Instrumentación Científica (CIC) of the University of Granada.

Appendix A. Supporting information

Supplementary data associated with this article can be found in the online version at [doi:10.1016/j.conbuildmat.2024.138713](https://doi.org/10.1016/j.conbuildmat.2024.138713).

Data availability

Data will be made available on request.

References

- O. Ortiz, F. Castells, G. Sonnemann, Sustainability in the construction industry: a review of recent developments based on LCA, *Constr. Build. Mat.* 23 (2009) 28–39.
- N. Lushnikova, L. Dvorkin, Sustainability of Gypsum Products as A Construction Material, in: J.M. Khatib (Ed.), *Sustainability of Construction Materials*, Woodhead Publishing Series in Civil and Structural Engineering: Number, 17, Elsevier, Amsterdam, 2016, pp. 643–681.
- R.H. Geraldo, S.M. Pinheiro, J.S. Silva, H.M. Andrade, J. Dweck, J.P. Gonçalves, G. Camarini, Gypsum plaster waste recycling: a potential environmental and industrial solution, *J. Clean. Prod.* 164 (2017) 288–300.
- B. Middendorf, Physico-mechanical and microstructural characteristics of historic and restoration mortars based on gypsum: current knowledge and perspective, *Geol. Soc. Lond. Spec. Publ.* 205 (2002) 165–176.
- R.A. Kuntze, *Gypsum: Connecting Science and Technology (MNL 67)*, ASTM International, Newburyport, 2009.
- P. Bel-Anzué, K. Elert, Changes in traditional building materials: the case of gypsum in Northern Spain, *Archaeol. Anthropol. Sci.* 13 (2021) 1–17.
- D.Sanz Arauz, *Análisis del yeso empleado en revestimientos exteriores mediante técnicas geológicas*, PhD Thesis, Universidad Politécnica, Madrid (2009).
- F. Vegas, C. Mileto, F. Fratini, S. Rescic, May a building stand upon gypsum structural walls and pillars? The use of masonry made of gypsum in traditional architecture in Spain, in: W. Jäger, B. Haseltine, A. Fried (Eds.), *Proceedings of the 8th International Masonry Conference, International Masonry Society and Technische Universität Dresden*, 4–7, July 2010, pp. 2183–2219.
- M.T. Freire, M. do Rosário Veiga, A.S. Silva, J. de Brito, Studies in ancient gypsum based plasters towards their repair: physical and mechanical properties, *Constr. Build. Mater.* 202 (2019) 319–331.
- C. Rodríguez-Navarro, E. Ruiz-Agudo, A.B. Rodríguez-Navarro, M. Ortega-Huertas, Thermal decomposition of calcite: mechanisms of formation and textural evolution of CaO nanocrystals, *Am. Mineral.* 94 (2009) 578–593.
- A. Shvarzman, K. Kovler, G.S. Grader, G.E. Shter, The effect of dehydroxylation/amorphization degree on pozzolanic activity of kaolinite, *Cem. Concr. Res.* 33 (2003) 405–416.
- S. Kumar, Fly ash-lime-phosphogypsum cementitious binder: a new trend in bricks, *Mater. Struct.* 33 (2000) 59–64.
- S. Marinkovic, A. Kostic-Pulek, Examination of the system fly ash–lime–calcined gypsum–water, *J. Phys. Chem. Solids* 68 (2007) 1121–1125.
- I. Demir, M.S. Baspinar, Effect of silica fume and expanded perlite addition on the technical properties of the fly ash–lime–gypsum mixture, *Constr. Build. Mater.* 22 (2008) 1299–1304.
- A. Vimmrová, M. Keppert, O. Michalko, R. Černý, Calcined gypsum–lime–metakaolin binders: design of optimal composition, *Cem. Concr. Compos.* 52 (2014) 91–96.
- M. Doleželová, L. Scheinherrová, A. Vimmrová, Moisture Resistance and Durability of the Ternary Gypsum-based Binders, in: *Materials Science Forum*, Vol. 824, Trans Tech Publications Ltd, Suiza, 2015, pp. 81–87.
- T.A.M. da Cruz, R.H. Geraldo, A.R.D. Costa, K.R.D. Maciel, J.P. Gonçalves, G. Camarini, Microstructural and mineralogical compositions of metakaolin-lime-recycled gypsum plaster ternary systems, *J. Build. Eng.* 47 (2022) 103770.
- A. Çolak, The long-term durability performance of gypsum-Portland cement-natural pozzolan blends, *Cem. Concr. Res.* 32 (2002) 109–115.
- A.R.D. Costa, S.R.C. Matos, G. Camarini, J.P. Gonçalves, Hydration of sustainable ternary cements containing phosphogypsum, *Sustain. Mater. Technol.* 28 (2021) e00280.
- M.S. Morsy, S.H. Alsayed, Y.A. Salloum, Development of eco-friendly binder using metakaolin-fly ash–lime-anhydrous gypsum, *Constr. Build. Mater.* 35 (2012) 772–777.
- AENOR, U.N.E.-E.N. 13279-1, *Yesos de construcción y conglomerantes a base de yeso para la construcción. Parte 1, Definiciones y especificaciones*, Madrid, 2009.
- AENOR, UNE-EN 459-1, *Cales para la construcción. Parte 1: Definiciones, especificaciones y criterios de conformidad*, Madrid, 2016.
- M. Schmidt, H. Poellmann, A. Egersdoerfer, The use of a recycled glass powder and expanded glass containing metakaolin in different binder systems, in: *34th International Conference on Cement Microscopy*, Curran Associates Inc., Red Hook (NY), 2012, pp.350-397.
- Q.L. Yu, H.J.H. Brouwers, Microstructure and mechanical properties of β -hemihydrate produced gypsum: an insight from its hydration process, *Constr. Build. Mater.* 25 (2011) 3149–3157.
- S. Steiner, B. Lothenbach, T. Proseke, A. Borgschulte, F. Winnefeld, Effect of relative humidity on the carbonation rate of portlandite, calcium silicate hydrates and ettringite, *Cem. Concr. Res.* 135 (2020) 106116.
- J.I. Alvarez, R. Veiga, S. Martínez-Ramírez, M. Secco, P. Faria, N. Pagona Maravelaki, M. Ramesh, I. Papayianni, J. Válek, RILEM TC 277-LHS report: a review on the mechanisms of setting and hardening of lime-based binding systems, *Mater. Struct.* 54 (2) (2021) 63.
- J.D. Martin, *Using X Powder: a software package for Powder X-Ray diffraction analysis (GR, 1001/04, ISBN 84–609–1497–6)* 2004.
- AENOR, U.N.E.-E.N. 15803, *Conservación del patrimonio cultural. Métodos de ensayo. Determinación de la permeabilidad al vapor de agua (dp)*, Madrid, 2010.
- A.E. Charola, S.A. Centeno, Analysis of gypsum-containing lime mortars: possible errors due to the use of different drying conditions, *J. Am. Inst. Conserv.* 41 (2002) 269–278.
- AENOR, UNE-EN 1015-11, *Métodos de ensayo de los morteros para albañilería. Parte 11, Determinación de la resistencia a flexión y a compresión del mortero endurecido*, Madrid, 2020.
- D. Leeb, *Dynamic hardness testing of metallic materials*, *NDT Int.* 12 (1979) 274–278.
- K. Elert, R. Alabarce Alaminos, C. Benavides-Reyes, M. Burgos-Ruiz, The effect of lime addition on weathering resistance and mechanical strength of gypsum plasters and renders, *Cem. Concr. Compos.* 139 (2023) 105012.
- M. Mishmastehi, A.E. Van Driessche, G.J. Smales, A. Moya, T.M. Stawski, Advanced materials engineering in historical gypsum plaster formulations, *Proc. Natl. Acad. Sci.* 120 (2023) e2208836120.
- H. Nguyen, V. Carvelli, W. Kunther, M. Illikainen, P. Kinnunen, Phase evolution and mechanical performance of an ettringite-based binder during hydrothermal aging, *Cem. Concr. Res.* 143 (2021) 106403.
- J.E. Aubert, P. Segui, B. Husson, M. Measson, A method developed to quantify lime and gypsum consumed by mineral additions, *Cem. Concr. Compos.* 34 (2012) 874–880.
- M.D. Jackson, E.N. Landis, P.F. Brune, M. Vitti, H. Chen, Q. Li, A.R. Ingraffea, Mechanical resilience and cementitious processes in Imperial Roman architectural mortar, *Proc. Natl. Acad. Sci.* 111 (2014) 18484–18489.
- M. Frias, J. Cabrera, Influence of MK on the reaction kinetics in MK/lime and MK-blended cement systems at 20C, *Cem. Concr. Res.* 31 (2001) 519–527.
- K. Elert, E.S. Pardo, C. Rodríguez-Navarro, Alkaline activation as an alternative method for the consolidation of earthen architecture, *J. Cult. Herit.* 16 (2015) 461–469.

- [39] P.K. Mehta, Effect of lime on hydration of pastes containing gypsum and calcium aluminates or calcium sulfoaluminate, *J. Am. Ceram. Soc.* 56 (1973) 315–319.
- [40] L. Jossierand, O. Coussy, F. de Larrard, Bleeding of concrete as an ageing consolidation process, *Cem. Concr. Res.* 36 (2006) 1603–1608.
- [41] R.S. Berns, *Principles of Color Technology*, Wiley-Blackwell, Hoboken, 2000.
- [42] H.R. Sasse, R. Snethlage, Methods for the evaluation of stone consolidation treatments, in: N.S. Baer, R. Snethlage (Eds.), *Saving Our Architectural Heritage. The Conservation of Historic Stone Structures*, John Wiley & Sons Ltd, Chichester, 1997, pp. 223–243.
- [43] ASTM C28/C28M - 10, Specification for Gypsum Plasters, ASTM Headquarters, Conshohocken, PA, USA, 2020.
- [44] T.A. Fode, Y.A.C. Jande, T. Kivevele, Effects of raw and different calcined bentonite on durability and mechanical properties of cement composite material, *Case Stud. Constr. Mater.* (2024) e03012.
- [45] M. Murat, A. Attari, Modification of some physical properties of gypsum plaster by addition of clay minerals, *Cem. Concr. Res.* 21 (1991) 378–387.
- [46] M. Khayet, A. Velázquez, J.I. Mengual, Modelling mass transport through a porous partition: effect of pore size distribution, *J. Non-Equilib. Thermodyn.* 29 (2004) 279–299.
- [47] M. Krus, *Moisture Transport and Storage Coefficients of Porous Mineral Building Materials. Theoretical Principles and New Test Methods*, Fraunhofer IRB Verlag, Stuttgart, 1996.
- [48] J. Karni, E. Karni, Gypsum in construction: origin and properties, *Mater. Struct.* 28 (1995) 92–100.
- [49] P. Ayogu, M. Ezugwu, F. Eze, Principle of common-ion effect and its application in chemistry: a review, *J. Chem. Let.* 1 (2020) 77–83.
- [50] A. Klimchouk, The dissolution and conversion of gypsum and anhydrite, *Int. J. Speleol.* (1996) 21–36.
- [51] X. Chen, Q. Wang, Q. Wu, X. Xie, S. Tang, G. Yang, L. Luo, H. Yuan, Hydration reaction and microstructural characteristics of hemihydrate phosphogypsum with variable pH, *Constr. Build. Mater.* 316 (2022) 125891.
- [52] K. Liu, M. Deng, L. Mo, Influence of pH on the formation of gypsum in cement materials during sulfate attack, *Adv. Cem. Res.* 27 (2015) 487–493.
- [53] Y.W. Wang, F.C. Meldrum, Additives stabilize calcium sulfate hemihydrate (bassanite) in solution, *J. Mater. Chem.* 22 (2012) 22055–22062.
- [54] L. Fernández-Dfáz, Á. Fernández-González, M. Prieto, The role of sulfate groups in controlling CaCO₃ polymorphism, *Geochem. Cosmochim. Acta* 74 (2010) 6064–6076.
- [55] L. Fernández-Dfáz, C.M. Pina, J.M. Astilleros, N. Sánchez-Pastor, The carbonatation of gypsum: pathways and pseudomorph formation, *Am. Mineral.* 94 (2009) 1223–1234.
- [56] M. Kitamura, Crystallization and transformation mechanism of calcium carbonate polymorphs and the effect of magnesium ion, *J. Colloid Interf. Sci.* 236 (2001) 318–327.
- [57] Z. Hu, D.Yulin Deng, Synthesis of needle-like aragonite from calcium chloride and sparingly soluble magnesium carbonate, *Powder Technol.* 140 (2004) 10–16.
- [58] M. Kellermeier, F. Glaab, R. Klein, E. Melero-Garcia, W. Kunz, J.M. García-Ruiz, The effect of silica on polymorphic precipitation of calcium carbonate: an on-line energy-dispersive X-ray diffraction (EDXRD) study, *Nanoscale* 5 (2013) 7054–7065.
- [59] D. Zhao, J.M. Williams, P. Hou, A.J. Moment, S. Kawashima, Stabilizing mechanisms of metastable vaterite in cement systems, *Cem. Concr. Res.* 178 (2024) 107441.
- [60] H.Y. Ghorab, E.A. Kishar, Studies on the stability of the calcium sulfoaluminate hydrates. Part 1: effect of temperature on the stability of ettringite in pure water, *Cem. Concr. Res.* 15 (1985) 93–99.
- [61] C. McCague, Y. Bai, Q. Zhou, P.A.M. Basheer, Effect of calcium sulfates on the early hydration of calcium sulfoaluminate cement and the stability of embedded aluminium, in: *Second International Symposium on Cement-Based Materials for Nuclear Wastes (NUWCCEM2014)*, Societe Francaise Denergie Nucleaire, 03-06 Jun 2014, Avignon, France, pp. 1–12.
- [62] M.D. Jackson, J.P. Oleson, J. Moon, Y. Zhang, H. Chen, M.T. Gudmundsson, Extreme durability in ancient Roman concretes, *Am. Ceram. Soc. Bull.* 97 (2018) 22–28.
- [63] H.J. Yim, J.H. Kim, H.G. Kwak, J.K. Kim, Evaluation of internal bleeding in concrete using a self-weight bleeding test, *Cem. Concr. Res.* 53 (2013) 18–24.
- [64] J. Ducasse-Lapeyrusse, V. Vergès-Belmin, Traditional gypsum renders in the Paris area: focus on a particular typology, *Mater. Struct.* 54 (2021) 1–15.
- [65] C. Rodriguez-Navarro, E. Doehne, Salt weathering: influence of evaporation rate, supersaturation and crystallization pattern, *Earth Surf. Process. Landf.* 24 (1999) 191–209.
- [66] K. Elert, R.M. García Sánchez, C. Benavides-Reyes, F.L. Ordóñez, Influence of animal glue on mineralogy, strength and weathering resistance of lime plasters, *Constr. Build. Mater.* 226 (2019) 625–635.
- [67] C. Rodriguez-Navarro, A. Suzuki, E. Ruiz-Agudo, Alcohol dispersions of calcium hydroxide nanoparticles for stone conservation, *Langmuir* 29 (2013) 11457–11470.
- [68] F. Wu, X. You, M. Wang, T. Liu, B. Lu, G. Hou, R. Jiang, C. Shi, Increasing flexural strength of CO₂ cured cement paste by CaCO₃ polymorph control, *Cem. Concr. Compos.* 141 (2023) 105128.
- [69] J. de Brito, I. Flores-Colen, Renders, in: M.C. Gonçalves, F. Margarido (Eds.), *Materials for Construction and Civil Engineering: Science, Processing, and Design*, Springer, Switzerland, 2015, pp. 53–122.
- [70] AENOR, UNE-EN 998-1a Especificaciones de los morteros para albañilería. Parte 1. Morteros para revoco y enlucido, Madrid, 2010.
- [71] S. Bastianoni, A. Galli, V. Niccolucci, R.M. Pulselli, The ecological footprint of building construction, in: U. Mander, C.A. Brebbia, E. Tiezzi (Eds.), *The Sustainable City IV: Urban Regeneration and Sustainability*, 93, WIT Transactions on Ecology and the Environment, 2006, pp. 345–356.
- [72] G. Hammond, C. Jones, *Inventory of carbon & energy: ICE. Vol. 5. Bath*, in: UK: Sustainable Energy Research Team, Department of Mechanical Engineering, University of Bath, 2008.
- [73] A.A. Abadel, A.S. Albidah, A.H. Altheeb, F.A. Alrshoudi, H. Abbas, Y.A. Al-Salloum, Effect of molar ratios on strength, microstructure & embodied energy of metakaolin geopolymer, *Adv. Concr. Constr.* 11 (2021) 127–140.
- [74] D.M. Martinez, A. Horvath, P.J. Monteiro, Comparative environmental assessment of limestone calcined clay cements and typical blended cements, *Environ. Res. Commun.* 5 (2023) 055002.
- [75] M. Mahboob, M. Ali, T.U. Rashid, R. Hassan, Assessment of embodied energy and environmental impact of sustainable building materials and technologies for residential sector, *Eng. Proc.* 12 (2021) 62.
- [76] Y. Florentin, D. Pearlmutter, B. Givoni, E. Gal, A life-cycle energy and carbon analysis of hemp-lime bio-composite building materials, *Energy Build.* 156 (2017) 293–305.
- [77] B. Lawson, D. Rudder, *Building Materials Energy and the Environment: Towards Ecologically Sustainable Development*, Royal Australian Institute of Architects, Canberra, 1996.